Exploring the representation of the far-field radiation pattern of an SKA antenna as a series expansion in terms of spherical harmonic basis functions

Modhurita Mitra and Athol Kemball

Department of Astronomy, 1002 W. Green Street,
University of Illinois at Urbana-Champaign, Urbana, IL 61801

ABSTRACT

In this memo, we explore the representation of the radiation pattern of an SKA antenna as an expansion, up to a certain degree, of scalar spherical harmonic functions with vector coefficients. This is done in an effort to compactly represent the antenna radiation pattern in terms of a few parameters, and hence decrease the computer memory that would be required to store the radiation pattern at finely sampled position angles.

1. Introduction

In order to increase the sensitivity of the SKA, it is important to subtract out the contribution from the sidelobes in the antenna radiation pattern. In order to suppress the sidelobe contribution accurately, we have to know the radiation pattern very precisely. One way to achieve this is to specify the electric field at very closely spaced points in (θ, ϕ). In this memo we investigate if we can instead represent the electric as an expansion in terms of a suitable set of basis functions up to a certain degree and reduce the number of parameters required to represent the field.

Traditionally, vector spherical harmonic basis functions with scalar coefficients have been used to represent the radiation pattern of an antenna (J. D. Jackson 1999). More recently, Rahola *et al.* (2009) have used scalar spherical harmonic basis functions with vector coefficients to represent the radiation pattern. We follow the approach of Rahola *et al.* (2009) and investigate whether the electric field data for an SKA antenna can be compactly represented in terms of expansion up to a certain degree of scalar spherical harmonic basis functions with vector coefficients.

The spherical harmonic of order m and degree l is given by (Rahola *et al.* 2008)

$$Y_l^m(\theta,\phi) = b_{lm} P_l^m(\cos\theta) e^{im\phi} \tag{1}$$

Here, $P_l^m(\cos\theta)$ is the associated Legendre polynomial of order m and degree l, and b_{lm} is the normalization coefficient which makes the spherical harmonics an orthonormal set of basis functions in two dimensions.

The far-field of the antenna radiation pattern can be expressed in terms of a linear combination of spherical harmonics with vector coefficients $\mathbf{a}_{lm}$ as (Rahola *et al.* 2008, 2009)

$$\mathbf{E}(\hat{\mathbf{r}}) = \sum_{l=0}^{\infty} \sum_{m=-l}^{l} \mathbf{a}_{lm} Y_l^m(\hat{\mathbf{r}}) \tag{2}$$

where $\hat{\mathbf{r}} = \hat{\mathbf{r}}(\theta,\phi) = (\sin\theta\cos\phi, \sin\theta\sin\phi, \cos\phi)$ is the unit vector to the direction represented by (θ,ϕ).

In this memo, we use the terms radiation pattern, beam pattern, and electric field pattern interchangeably.

2. Calculation of Spherical Harmonic Coefficients

The far-field radiation pattern data has been obtained from optical experiments and numerical simulations. The measured radiation pattern data is provided in the form $(\mathbf{E}_{\hat{\theta}}(\theta,\phi), \mathbf{E}_{\hat{\phi}}(\theta,\phi))$, i.e., the amplitudes and phases of the electric field in the $\hat{\theta}$ and $\hat{\phi}$ directions are provided at the sampling points in (θ,ϕ). The electric field is sampled every 0.2 degree in θ and every 1 degree in ϕ.

The measured radiation pattern is shown in Figure 1, in which the real and imaginary parts and the magnitude of the forward beam pattern (θ = 0 to 90 degrees) are shown as false-color images in the (l,m) plane. Only the central region of the (l,m) plane ($-0.15 \leq l \leq 0.15, -0.15 \leq m \leq 0.15$) is displayed in the images. The evenly spaced sample points in (θ,ϕ) map to unevenly spaced points in the (l,m) plane; therefore, interpolation and gridding were used to obtain data at evenly spaced points in the (l,m) plane. All the false-color images in this memo are obtained and displayed in this same manner.

To calculate the vector spherical harmonic coefficients, we first convert this data from spherical coordinates to Cartesian coordinates. We closely follow the approach and notation of Rahola *et al.* (2008, 2009), with some minor changes.

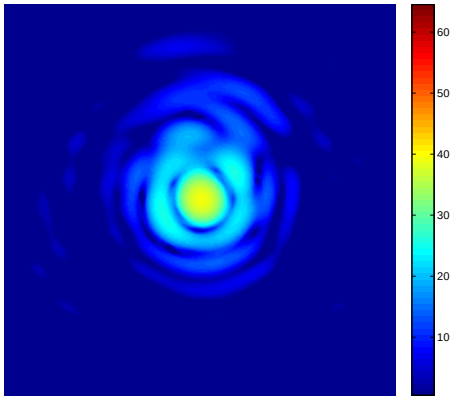

Real Part

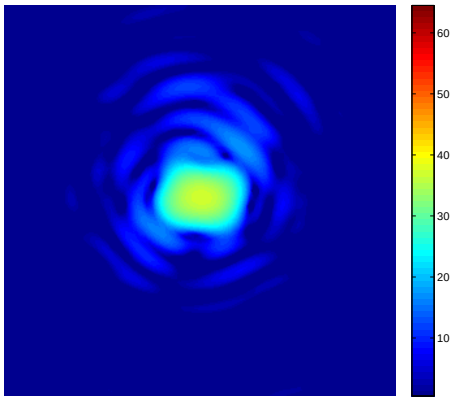

Imaginary Part

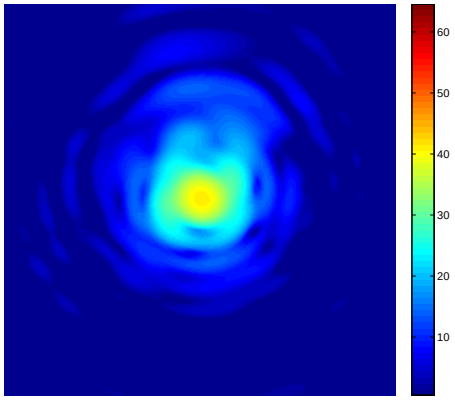

Magnitude

Fig. 1.— Real and imaginary parts, and magnitude, of the measured radiation pattern in the central part of the (l, m) plane; l ranges from -0.15 to 0.15, increasing from left to right, m ranges from -0.15 to 0.15, increasing from bottom to top.

The electric field data in spherical coordinates is given in the form

$$\mathbf{E}_s(\hat{\mathbf{r}}_k) = [E_\phi(\hat{\mathbf{r}}_k) \quad E_\theta(\hat{\mathbf{r}}_k)]^T \tag{3}$$

at K points given by $\hat{\mathbf{r}}_k = (\theta_k, \phi_k)$. To find the Cartesian components of the electric field,

$$\mathbf{E}_c(\hat{\mathbf{r}}_k) = [E_x(\hat{\mathbf{r}}_k) \quad E_y(\hat{\mathbf{r}}_k) \quad E_z(\hat{\mathbf{r}}_k)]^T \,, \tag{4}$$

we use the transformation equation

$$\mathbf{E}_c(\hat{\mathbf{r}}_k) = \mathbf{T}(\hat{\mathbf{r}}_k)\mathbf{E}_s(\hat{\mathbf{r}}_k) \,, \tag{5}$$

where the transformation matrix $\mathbf{T}(\hat{\mathbf{r}})$ is given by

$$\mathbf{T}(\hat{\mathbf{r}}) = \begin{bmatrix} -\sin\phi & \cos\phi & 0 \\ \cos\theta\cos\phi & \cos\theta\sin\phi & -\sin\theta \end{bmatrix}^T \tag{6}$$

Given the electric field $\mathbf{E}(\hat{\mathbf{r}})$ in Equation 2, the coefficients $\mathbf{a}_{lm}$ can be found by integrating the radiation pattern $\mathbf{E}(\hat{\mathbf{r}})$ with the spherical harmonics, exploiting the orthonormality property of spherical harmonics (Rahola *et al.* 2008). Alternatively, a least squares approach can be used to solve the linear system of equations given by Equation (2) (Rahola *et al.* 2008, 2009). We describe both these methods in the following subsections.

2.1. Integration Method

The spherical harmonic basis functions given by Equation (1) are orthonormal:

$$\int_\Omega Y_l^m(\hat{\mathbf{r}}) Y_{l'}^{m'*}(\hat{\mathbf{r}}) \, d\Omega = \delta(l - l', m - m') \,. \tag{7}$$

where Ω is the solid angle and the integration is over the unit sphere. This can be rewritten as

$$\int_0^{2\pi} \int_0^{\pi} Y_l^m(\theta, \phi) Y_{l'}^{m'*}(\theta, \phi) \sin\theta \, d\theta \, d\phi = \delta(l - l', m - m') \,. \tag{8}$$

Therefore, from Equations (2) and (7), the vector spherical harmonic expansion coefficient $\mathbf{a}_{lm}$ can be found by multiplying the radiation pattern $\mathbf{E}(\hat{\mathbf{r}})$ by the complex conjugate $Y_l^{m*}(\hat{\mathbf{r}})$ of the corresponding spherical harmonic basis function $Y_l^m(\hat{\mathbf{r}})$, and integrating over the unit sphere:

$$\mathbf{a}_{lm} = \int_{\Omega} \mathbf{E}(\hat{\mathbf{r}}) Y_l^{m*}(\hat{\mathbf{r}}) d\Omega \,, \tag{9}$$

which can be rewritten as

$$\mathbf{a}_{lm} = \int_0^{2\pi} \int_0^{\pi} \mathbf{E}(\theta, \phi) Y_l^{m*}(\theta, \phi) \sin\theta \, d\theta \, d\phi \,. \tag{10}$$

If the radiation pattern $\mathbf{E}(\hat{\mathbf{r}})$ is expressed in Cartesian coordinates as in Equation (4), Equation (10) is reduced to a set of three scalar equations

$$\begin{aligned} a_{x,lm} &= \int_0^{2\pi} \int_0^{\pi} E_x(\theta, \phi) Y_l^{m*}(\theta, \phi) \sin\theta \, d\theta \, d\phi \\ a_{y,lm} &= \int_0^{2\pi} \int_0^{\pi} E_y(\theta, \phi) Y_l^{m*}(\theta, \phi) \sin\theta \, d\theta \, d\phi \\ a_{z,lm} &= \int_0^{2\pi} \int_0^{\pi} E_z(\theta, \phi) Y_l^{m*}(\theta, \phi) \sin\theta \, d\theta \, d\phi \end{aligned} \tag{11}$$

where $\mathbf{a}_{lm} = [a_{x,lm},\, a_{y,lm},\, a_{z,lm}]^T$.

2.2. Linear Least Squares Method

For a given measurement point $\hat{\mathbf{r}}$, the set of spherical harmonics can be written as a vector

$$\mathbf{y}(\hat{\mathbf{r}}) = [\mathbf{y}_0(\hat{\mathbf{r}}),\, \mathbf{y}_1(\hat{\mathbf{r}}),\, \ldots,\, \mathbf{y}_L(\hat{\mathbf{r}})] \tag{12}$$

where L is the highest degree of expansion and

$$\mathbf{y}_l(\hat{\mathbf{r}}) = [\mathbf{Y}^l_{-l}(\hat{\mathbf{r}}),\, \mathbf{Y}^l_{-l+1}(\hat{\mathbf{r}}),\, \ldots,\, \mathbf{Y}^l_{-1}(\hat{\mathbf{r}}),\, \mathbf{Y}^l_0(\hat{\mathbf{r}}),\, \mathbf{Y}^l_1(\hat{\mathbf{r}}),\, \ldots, \mathbf{Y}^l_{l-1}(\hat{\mathbf{r}}),\, \mathbf{Y}^l_l(\hat{\mathbf{r}})] \tag{13}$$

represents the set of spherical harmonics at degree l.

The spherical harmonics at all K measurement points can be collected in the matrix

$$\mathbf{Y} = [\mathbf{y}^T(\hat{\mathbf{r_1}}),\, \ldots,\, \mathbf{y}^T(\hat{\mathbf{r_K}})] \tag{14}$$

and the measured electric field in Cartesian coordinates at all K measurement points can be represented as the matrix

$$\mathbf{F}_c = [\mathbf{E}_c(\hat{\mathbf{r_1}}),\, \ldots,\, \mathbf{E}_c(\hat{\mathbf{r_K}})] \tag{15}$$

The matrix

$$\mathbf{A} = [\mathbf{a}_x,\, \mathbf{a}_y,\, \mathbf{a}_z] \tag{16}$$

is defined to contain the spherical harmonic coefficients. Then the measured field in Cartesian coordinates, $\mathbf{F}_c$, is related to the matrix of spherical harmonics, $\mathbf{Y}$, through the equation

$$\mathbf{F}_c = \mathbf{A}\mathbf{Y} \tag{17}$$

This equation represents the noise-free case. In the typical case of noisy measurements, the measured field is of the form

$$\tilde{\mathbf{F}}_c = \mathbf{A}\mathbf{Y} + \mathbf{N}\,, \tag{18}$$

where $\mathbf{N}$ is the measurement noise.

A least-squares estimate of $\mathbf{A}$ is then given by

$$\hat{\mathbf{A}} = \arg\min_{\mathbf{A}} ||\tilde{\mathbf{F}}_c - \mathbf{A}\mathbf{Y}||_F^2 \tag{19}$$

where $||\cdot||_F$ denotes the Frobenius norm.

The least-squares problem described by Equation (19) can be solved by calculating the Moore-Penrose pseudoinverse ($\mathbf{Y}^\dagger$) of $\mathbf{Y}$. $\hat{\mathbf{A}}$ is then given by

$$\hat{\mathbf{A}} = \tilde{\mathbf{F}}_c \mathbf{Y}^\dagger \tag{20}$$

2.3. Comparison of the two methods

In the integration method, each spherical harmonic expansion coefficient is computed separately, independent of other coefficients. However, the data need to be complete and sampled closely for the integration to yield correct values of the coefficients (Rahola *et al.* 2008). The accuracy of the results obtained using this method is limited by discretization errors, numerical integration errors, and the measurement errors in the noisy data.

For spherical harmonic expansion degree L, the total number of coefficients is $(L+1)^2$ for each Cartesian coordinate direction. Therefore, the least squares method involves solving jointly for $(L+1)^2$ variables. Also, in the case of noisy data, the number of data samples K must be much greater than the number of variables $(L+1)^2$ in order to form an overdetermined system of equations which can yield robust solutions for the values of the coefficients (Rahola *et al.* 2009). When the radiation pattern has a complex structure, a large number of coefficients are required to represent it. In that case, the least squares method would involve the solution of a large system of linear equations, and could be computationally challenging. The accuracy of the results obtained using this method is limited by discretization errors, the sensitivity of the least squares solver used, and the measurement errors in the noisy data.

Rahola *et al.* (2009) used the linear least squares method since they wanted to be able to compute the coefficients from incomplete measurement data. However, we have very complete data - the radiation pattern data is provided at very closely sampled intervals, every 0.2 degree in θ and every 1 degree in ϕ. Also, we faced computational challenges while attempting to solve the problem using the least squares method. We have data at K=324,360 points, and we could not solve this problem for spherical harmonic expansion degree of even a few tens using serial computing; we would have needed parallel computing to solve this problem. Therefore, we decided to solve this problem using the integration method.

3. Results and Discussion

We calculated the simple harmonic expansion coefficients using the integration method described in the previous section. We used MATLAB to perform our computations.

We calculate $\mathbf{E}_{r,L}(\hat{\mathbf{r}})$, the reconstructed electric field computed by evaluating the series expansion given in Equation (2) till degree $l = L$, as follows:

$$\mathbf{E}_{r,L}(\hat{\mathbf{r}}) = \sum_{l=0}^{L} \sum_{m=-l}^{l} \mathbf{a}_{lm} Y_l^m(\hat{\mathbf{r}})\,. \tag{21}$$

We define the fractional error in the reconstructed electric field as

$$f(L) = \sqrt{\frac{\sum\limits_{\hat{\mathbf{r}}} |\mathbf{E}_{r,L}(\hat{\mathbf{r}}) - \mathbf{E}(\hat{\mathbf{r}})|^2}{\sum\limits_{\hat{\mathbf{r}}} |\mathbf{E}(\hat{\mathbf{r}})|^2}} \quad , \tag{22}$$

where $\mathbf{E}(\hat{\mathbf{r}})$ is the measured electric field and L is the expansion degree. The fractional error, $f(L)$, is plotted as a function of the expansion degree, L, in Figure 2. We observe that $f(L)$ decreases steadily with L till $L = 190$, at which point its value is $f(L) = 0.0189$, and then increases steadily with L. Therefore, the radiation pattern can be represented to an accuracy of 98.11% (1.89% error) using a series expansion in terms of spherical harmonic basis functions till degree $L = 190$. We believe that the residual 1.89% error is due to discretization effects, since the radiation pattern is not known below the sampling resolution of 0.2 degree in θ and 1 degree in ϕ. We also note that the plot in Figure 2 is linear for nearly the entire range between $L = 0$ and $L = 190$, with a slope $\sim 1/190 = 0.0053$. Therefore, the error in the reconstructed radiation pattern decreases at the rate of about half percent for every additional spherical harmonic expansion degree.

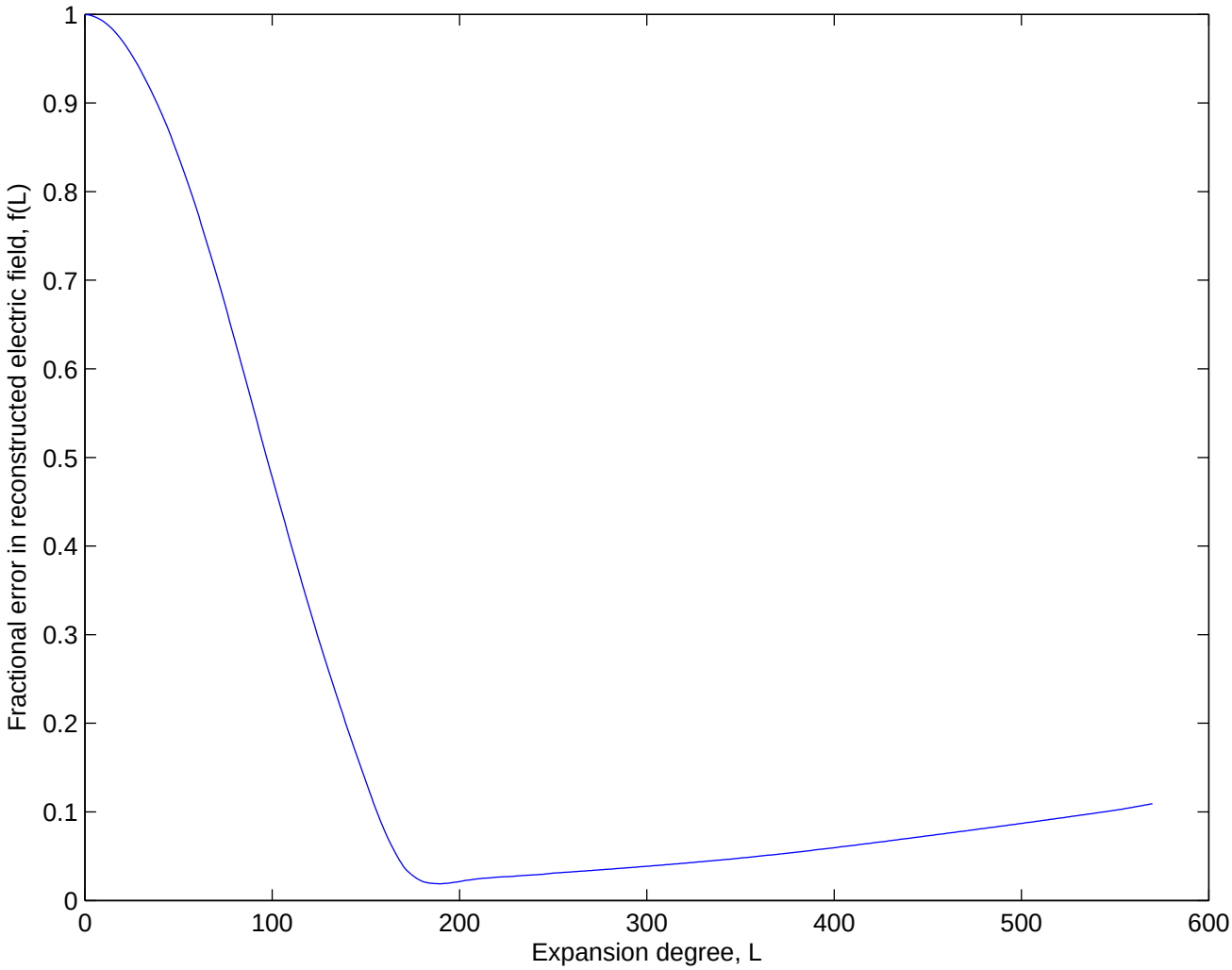

Fig. 2.— Relative error, $f(L)$, in the reconstructed electric field as a function of spherical harmonic expansion degree, L. See text for more details.

The total number of coefficients required for a series expansion till degree $L = 190$ is $(L+1)^2 = 36,481$, for each coordinate direction. This is 11.25% of the number of parameters (K=324,360) required to represent the electric field at each point, in each spatial direction. Therefore, at the expense of 1.89% error, we can represent the entire radiation pattern in terms of 11.25% of the number of parameters that would be required to represent the raw electric field data. This represents a savings of 88.75% in the amount of computer memory required to store the beam pattern.

The reconstructed radiation patterns, and the residuals between the reconstructed and measured radiation patterns, are shown in Figures 3 (real part), 4 (imaginary part), and 5 (magnitude), for a few illustrative values of the expansion degree L. As expected, with increasing L, the reconstructed radiation pattern approaches the measured pattern, and the residual approaches zero.

In conclusion, we have demonstrated that the provided SKA beam pattern can be described to an accuracy of 98.11% by representing it as a series expansion, till degree $L = 190$, of scalar spherical harmonic basis functions with vector coefficients. Representing the measured electric field pattern in this form yields a savings of 88.75% in the amount of computer memory required to store the beam pattern, compared to the memory that would be required to save the entire electric field pattern in its raw form.

REFERENCES

J. D. Jackson (1999). *Classical Electrodynamics*. John Wiley & Sons, Inc.

Rahola, J., Belloni, F., and Richter, A. (2008). Processing of radiation patterns using spherical harmonic expansions. In *Finnish National URSI Convention Radio Science/Electromagnetic, Espoo, Finland*.

Rahola, J., Belloni, F., and Richter, A. (2009). Modelling of radiation patterns using scalar spherical harmonics with vector coefficients. In *EuCAP 2009: 3rd European Conference on Antennas and Propagation*, pages 3361–3365.

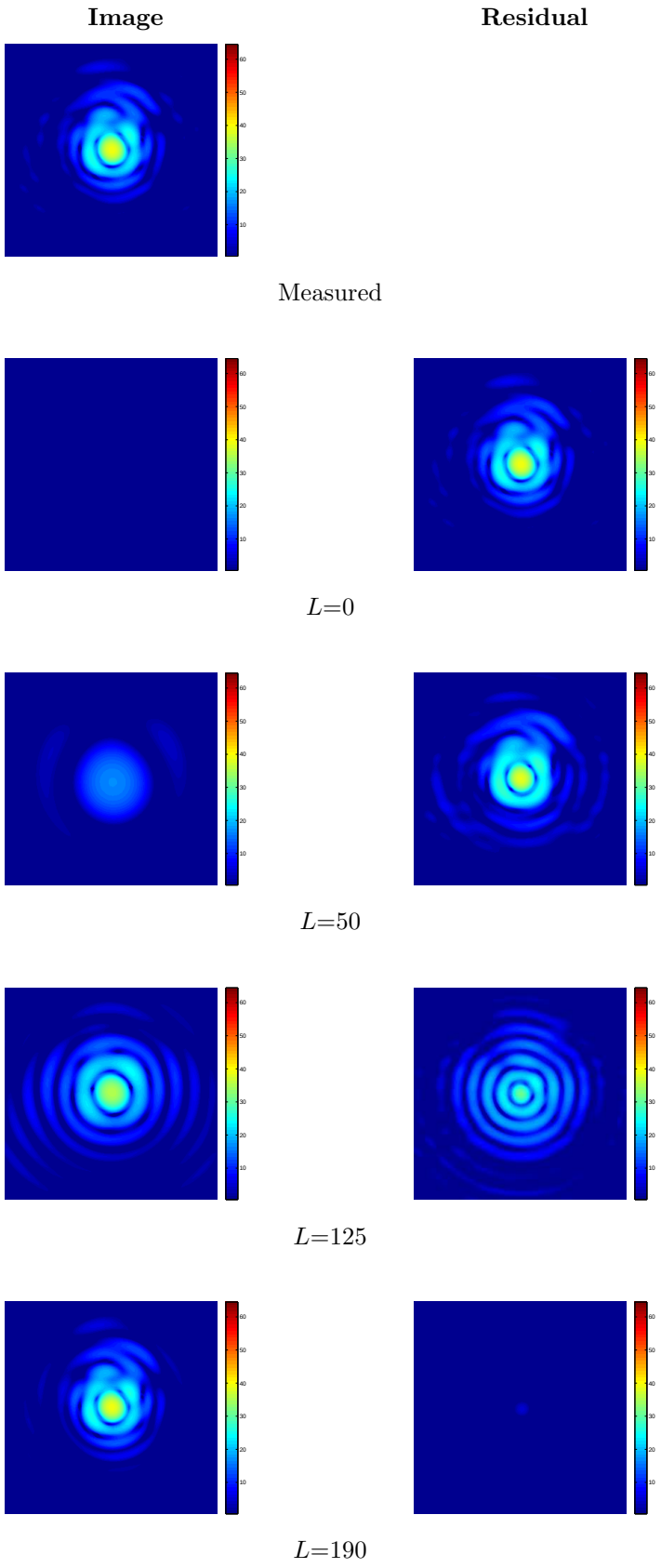

Fig. 3.— Real parts of measured and reconstructed images in the central part of the (l, m) plane, and the residual left after subtracting the reconstructed image from the measured image; l ranges from -0.15 to 0.15, increasing from left to right, m ranges from -0.15 to 0.15, increasing from bottom to top. L is the degree of the spherical harmonic expansion.

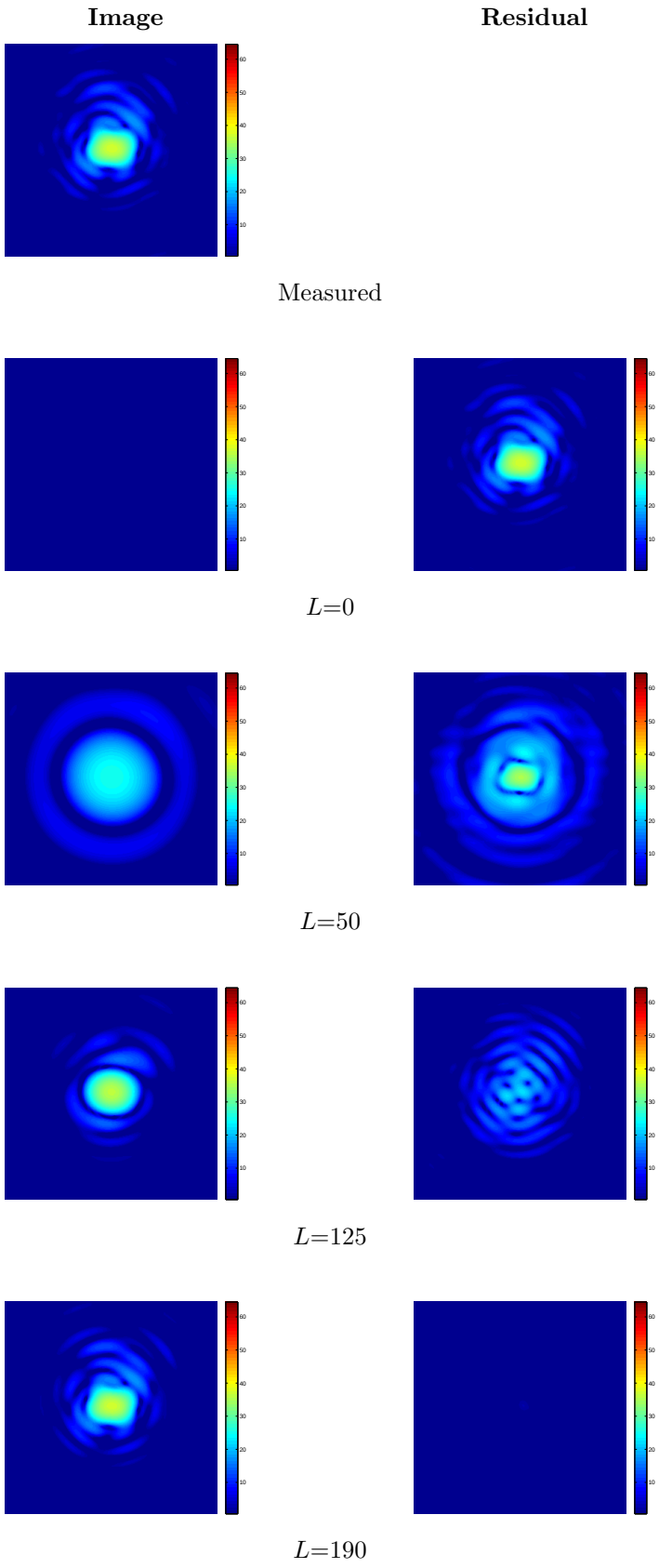

Fig. 4.— Imaginary parts of measured and reconstructed images in the central part of the (l, m) plane, and the residual left after subtracting the reconstructed image from the measured image; l ranges from -0.15 to 0.15, increasing from left to right, m ranges from -0.15 to 0.15, increasing from bottom to top. L is the degree of the spherical harmonic expansion.

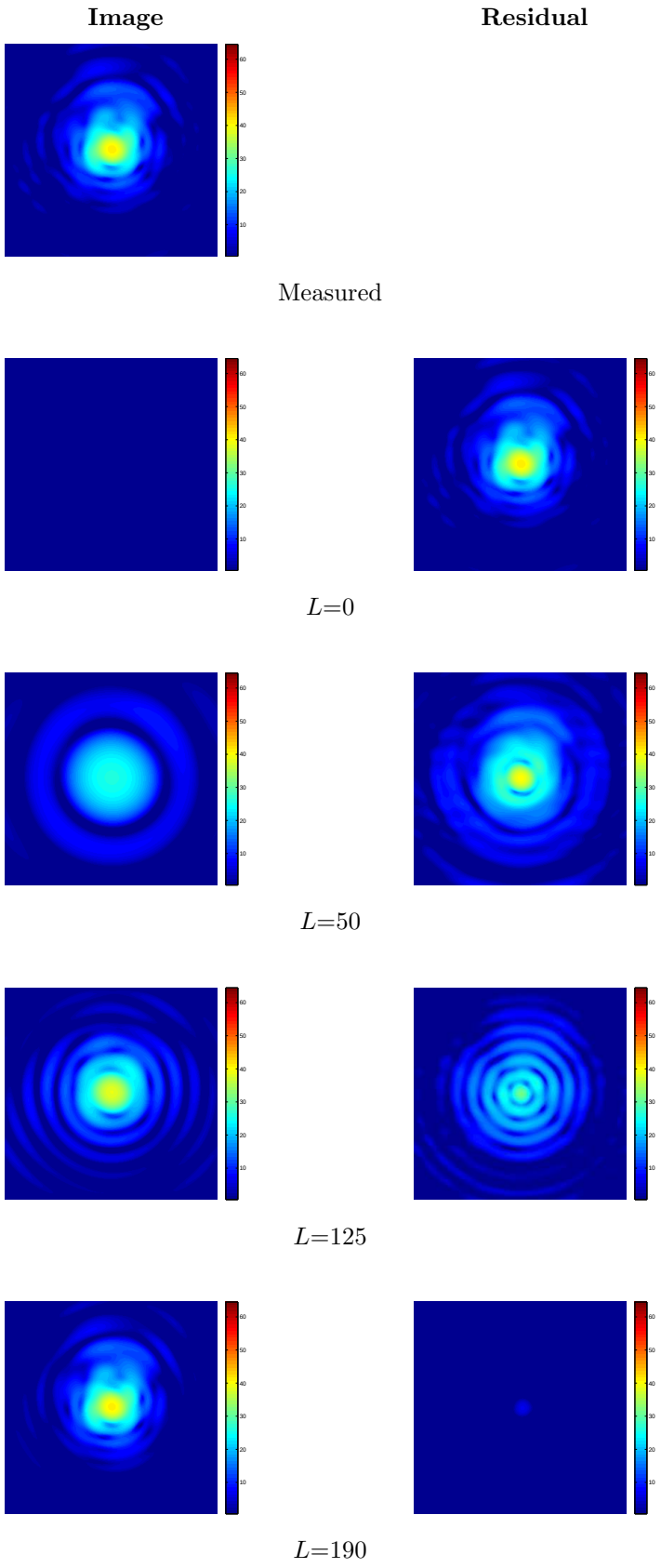

Fig. 5.— Magnitudes of measured and reconstructed images in the central part of the (l, m) plane, and the residual left after subtracting the reconstructed image from the measured image; l ranges from -0.15 to 0.15, increasing from left to right, m ranges from -0.15 to 0.15, increasing from bottom to top. L is the degree of the spherical harmonic expansion.